A Preconceptual Design of an Inverted Stable-Salt Reactor

Cihang Lu* and Zeyun Wu

Department of Mechanical and Nuclear Engineering, Virginia Commonwealth University
401 W. Main St., Richmond VA, USA 23284-3015

luc4@vcu.edu, zwu@vcu.edu

doi.org/10.13182/PHYSOR22-37487

ABSTRACT

This paper presents a preconceptual design of an inverted stable-salt reactor (SSR), with the unique feature that the static fuel salt is accommodated in one single bulk fuel container, while the coolant salt is circulating through the core via flow tubes penetrating the fuel container. The inverted SSR is expected to substantially decrease the capital cost compared to the state-of-the-art SSR such as the SSR–W designed by Moltex Energy, because one single gas vent at the top of the fuel container is required in the inverted SSR to prevent the leakage of the radioactive fission product gases instead of one gas vent in each of the hundreds of thousands of fuel tubes in SSR-W. In addition, the operation of the inverted SSR is largely simplified. However, numerous challenges associated with the design of the inverted SSR still remain to be overcome. Preliminary neutronics and thermal-hydraulics performance characteristics of the inverted SSR are assessed in this study. A viable core configuration of the inverted SSR is identified, and the superior characteristics of the inverted SSR, including a better neutron economy and a lower maximum fuel temperature, are demonstrated in this paper.

KEYWORDS: spent nuclear fuel, stable-salt reactor, inverted stable-salt reactor

1. INTRODUCTION

Nuclear energy is being pursued worldwide as a zero-CO_2-emission clean energy source. However, the employment of the convectional water-cooled reactors, which currently account for more than 95% of the operating civilian reactors fleet in the world, is inevitable accompanied by the generation of spent nuclear fuel (SNF) due to their thermal neutron spectra. The management of SNF is strictly regulated because of its high radioactivity. Although the dry-cast storage is aimed, most SNF is currently stored in specially designed nuclear waste pools at individual reactor sites due to the regulatory issues associated with transportation and permanent storage sites.

Besides storing the SNF, an alternative approach to tackle the waste before its permanent storage is to burn the higher actinide components in the SNF and leave only short-lived fission products in the waste stream by utilizing specifically designed reactors with the fast neutron spectra. The Stable-Salt Reactor–Wasteburner (SSR-W) [1], designed by Moltex Energy, is a representative design of these waste-burning

* Current address: Nuclear Science & Technology Department, Brookhaven National Laboratory (clu@bnl.gov)

reactors. The SSR–W is a molten-salt-fueled molten-salt-cooled reactor, with the unique feature of employing static molten salt fuel tubes, which are fabricated by replacing the solid pellets in conventional water-cooled-reactor-style fuel assemblies with molten salt fuel. By immobilizing the molten salt, the technical hurdles of managing a mobile molten salt fuel, faced in the conventional Molten Salt Reactor (MSR)-type reactors, are circumvented. As low-purity reactor-grade plutonium recycled from stocks of SNF produced by the Waste to Stable Salt (WATSS) process is proposed in the SSR-W design, the fuel cost is expected to be negative, thanks to the reduced liability cost for disposal of the SNF. Each fuel tube of the SSR-W is specially designed to have a diving bell gas vent at the top to avoid buildup of pressure in the fuel tube and to “hold up” fission product gases such that they can decay before being released. However, due to the large amount of fuel tubes employed (over 37,800 fuel tubes in one reactor module of 375 MWth power scale in Ref. [1]), the capital cost of the SSR-W may be high.

The Moltex SSR-W concept, which represents the most cutting-edge technique in the realm of SSR thus far, can be essentially considered to be derived from the solid fueled sodium fast reactors (SFRs). Therefore, it leverages the design advantages of both SFRs and MSRs. However, SSR inherited a complicated design paradigm similar to the SFR design (e.g., a conventional solid fueled fast reactor design scheme consisting fuel rod, fuel assembly, and reactor core design). Limited by this design pattern, the manufacturing challenge and cost of the SSR are envisioned to be high. For instance, the SRR fuel rod design (referred to as fuel tube in the Moltex technical reports) requires advances in manufacturing technique and tube material because of its small size in diameter (~1 cm) and containment of high temperature molten salt (~750 °C). Furthermore, SSR-W requires installing over 200 fuel assemblies with each assembly containing over 370 tightly packed fuel tubes together. These complicated configurations will make the fuel tube fabrication and the following assemble procedure of the SSR-W core be likely source of construction delays and cost overruns. Considering the foreseeable economic disadvantage of the SSR-W design, and also being inspired by the recent stationary liquid fuel fast reactor (SLFFR) design [2], this paper introduces a preconceptual design of an inverted SSR with a much-simplified core configuration aiming to decrease the capital cost. The inverted SSR design to reduce the complexity of the core configuration with the intension to reduce the total manufacturing cost of the reactor and accelerate the deployment of this innovative reactor concept. The simplicity of the inverted SSR design can be well explained by Fig. 1, which provides a schematic view of the inverted SSR design in a comparative manner to the Moltex SSR-W design.

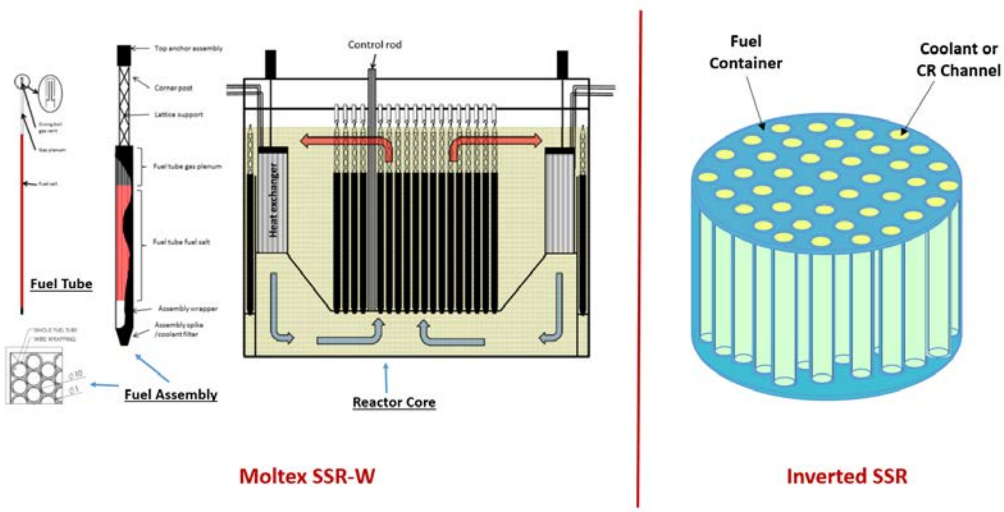

Figure 1. The schematic view of the Moltex SSR-W [1] and the inverted SSR design.

As shown in Fig. 1, the Moltex SSR-W design employs the traditional fast reactor heterogeneous design paradigm that requires fuel tube, fuel assembly and reactor core configuration. In the SSR-W design, the liquid fuel salt is completely contained in small diameter fuel tubes bound in the fuel assembly. The whole

SSR-W is composed of 200 fuel assemblies and is fully immersed in a non-radioactive molten salt pool, which provides heat removal capability by circulating the secondary coolant salt fluid through the assemblies. By contrast, in the inverted SSR design, the liquid fuel salt will be contained within a closed large volume container with penetrating coolant channels, and thus will neither be mixed with coolant salt nor flow through the primary heat transfer loop. The fuel container plays the role of conventional fuel cladding; thus, the defense-in-depth principle is retained as opposed to other flowing fluid fuel concepts. Because of this reason, this design is regarded an inverted version of the Moltex SSR design. However, the inverted SSR core is evolved to be a single integral homogeneous component, which significantly simplifies the core design and thus anticipates large cost reduction in manufacturing. Furthermore, the reactor will be designed to operate with an online-refueling system which will allow gaseous fission products to be removed continuously without the fuel shuffling and replacement scheme as required by SSR-W.

However, numerous challenges associated with the design of the inverted SSR still remain to be overcome. For example, the integration of the coolant channels to the fuel container needs to be tackled. Specifically designed fuel container can be fabricated with additive manufacturing to solve this problem, but limitations on coolant channel sizes and numbers may apply. Moreover, the flow of the fuel salt in the bulk fuel container needs to be investigated, for both normal operating conditions and accidental scenarios. Furthermore, the irradiation damage of the fuel container structure needs to be studied to come up with reasonable fuel container replacement strategies. The rest of paper summarizes a preliminary neutronics and thermal-hydraulics analysis of the preconceptual inverted SSR design. A viable core configuration of the inverted SSR is provided, and the superior performance characteristics of the inverted SSR, including a lower maximum fuel temperature and a better neutron economy, are demonstrated through the analysis.

2. NEUTRONICS PERFORMANCE ANALYSIS

Neutronics calculations of both the reference SSR-W and the inverted SSR are performed in this section by using the Monte Carlo neutronics code Serpent [3] with neutron cross section library ENDF/B-VII.1. All the Serpent calculations performed were two-dimensional (2-D) at this stage. The reactor cores were modeled to have a height of 1 cm, and a periodic boundary condition was applied on the z-axis direction. A temperature of 1200 K was assumed for the fuel material while a temperature of 900 K was assumed for all the other materials. For all the calculations, 200,000 particles were generated in each active cycle, and 100 active cycles were employed, which made the total active neutron history number 2×10^7. Each calculation was finished in around 15 minutes by using 45 processor cores, and the associated uncertainties of the k_{eff} obtained were smaller than 10 pcm.

2.1. Reference Core: SSR-W

The SSR-W designed is still under active research and improvements are being continuously incorporated into its design. In this paper, the neutronics model of the SSR-W was built according to the parameter descriptions from [1] and [4], which were published in 2018 and 2017, respectively. Although the neutronics model built in this paper may not reflect the state-of-the-art design of the SSR-W, it was adequate to provide reference calculations for the evaluation of the performance of the inverted SSR.

In the SSR-W neutronics model, four different materials were used. They are defined as follows:

- "Fuel" - The initial liquid fuel employed in the SSR-W consisted of 60 mol% of NaCl, 20 mol% of $PuCl_3$, and 20 mol% of UCl_3 (or $LnCl_3$), and is expected to be made from PuO_2, obtained from reprocessed conventional SNF, and depleted UCl_3 [4]. In this work, the uranium was modeled as pure ^{238}U for simplicity, and the abundance of different Pu isotopes in the SNF of typical pressurized water reactor (PWR) was obtained from ref. [5]. The fuel material was modeled at 1200 K, and the mass density was estimated from ref. [6] and ref. [7].

- "Coolant" - The coolant salt consisted of 48 mol% of KF, 10 mol% of NaF, 40 mol% of ZrF_4, and 2 mol% of ZrF_2 [4]. The coolant material was modeled at 900 K and considered to have a density of $2.77 g/cm^3$ [4]. It is pointed out that this fluoride-based coolant may be unfavorable for fast-spectrum breeder reactors due to the relatively good moderation capability of fluoride. Chloride-base coolant is therefore currently under active research for the SSR-W design.
- "HT-9 steel" - The chemical composition of HT-9 steel was obtained from ref. [8] and the density of HT-9 at 900 K was estimated according to ref. [9].
- "SS-316L SS" – The chemical composition of SS-316L stainless steel (SS) was obtained from ref. [10] and the density of SS-316L SS at 900 K was estimated according to ref. [11].

The fuel tubes employed in the SSR-W had a diameter of 1 cm, and the pitch between two tubes was 1.1 cm as each fuel tube had a 1-mm helical wire wrap. A square 18 × 21 hexagonal array of the fuel tubes was close packed in each fuel assembly [4]. Claddings of both the fuel tubes and the fuel assemblies, made of HT-9 steel, were assumed to have a thickness of 0.05 cm. At this stage, the helical wire wrap was not included in the neutronics model. A schematic of the fuel assemblies employed in the SSR-W [12] is shown in Fig. 2 in comparison with their 2-D Serpent neutronics model used in this work.

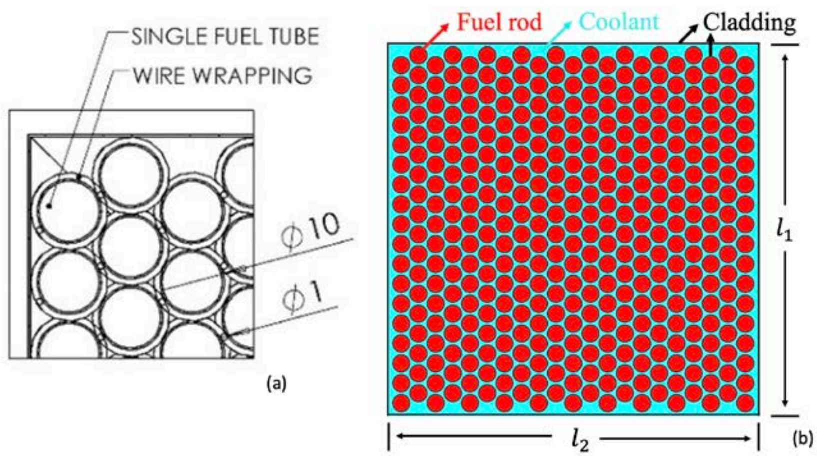

Figure 2. A schematic of (a) the SSR-W fuel assembly [12] and (b) its 2-D Serpent model.

Because the side lengths of the fuel assemblies of the SSR-W were not given in the literature, the following simple calculations were made to determine the minimum size of the fuel assemblies such that all the fuel rods can fit in. The side length l_1 and l_2 shown in Fig. 2(b) should satisfy

$$l_1 \geq 1.1cm \times \frac{1}{2} \times 35 + (0.5cm + 0.1cm) \times 2 = 20.45 \text{ cm}, \quad (1)$$

$$l_2 \geq 1.1cm \times \frac{\sqrt{3}}{2} \times 20 + (0.5cm + 0.1cm) \times 2 = 20.25 \text{ cm}, \quad (2)$$

The side length of the fuel assembly was therefore modeled as 20.45 cm in this work by assuming a square cross section of the fuel assemblies. An unusual design feature of the SSR-W is that its core is rectangular in shape [4]. Each fuel module contains 10 rows of 10 fuel assemblies and has a power of 375 MWth, and the total power of the SSR-W can be extended in its long dimension by adding additional modules [4]. A typical design of the SSR-W consists of two modules submerged in a pool of coolant with a length of 6 m and a width of 5 m [1], which is wrapped by a 2-meter-thick SS-316L SS wall that acts as both the reflector and the shielding [4]. A schematic of the SSR-W core and its 2-D Serpent neutronics model are shown in Fig. 3. The active core had a cross-sectional area of 84460 cm^2, and the k_{eff} was calculated as 1.44446 ± 0.00009. This large value of k_{eff} was caused by the ignorance of all the reactivity control systems in the neutronics model. Also, the fuel composition could be adjusted by performing a criticality search but is out of the scope of this study. The neutron spectrum in the SSR-W is plotted in Fig. 4 in comparison with that of the General Atomic (GA)'s 350 MWth MTHGR [13]. The difference in the neutron spectra clearly revealed the fast-spectrum nature of the SSR-W.

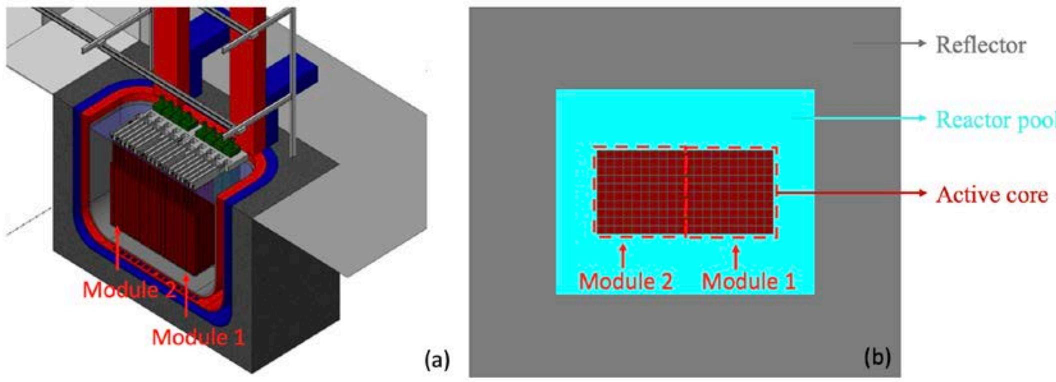

Figure 3. A schematic of (a) the SSR-W core [1] and (b) the 2-D Serpent model (top view).

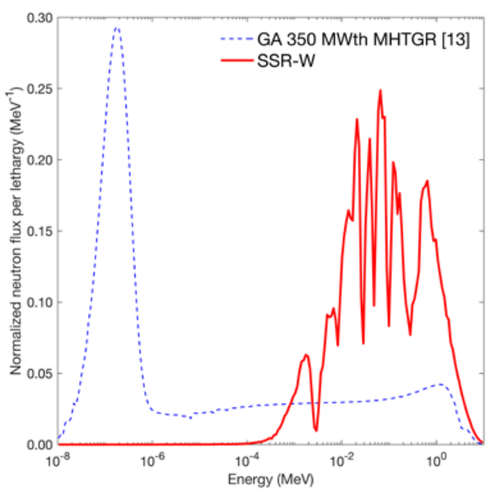

Figure 4. Comparison of neutron spectra in SSR-W with that in the GA's 350MWth HTGR [13].

2.2. Inverted SSR Core

The inverted SSR differs from the SSR-W that the static molten-salt fuel is accommodated in a bulk fuel container in the inverted SSR, while coolant channels are integrated to the bulk fuel container to provide a sufficient cooling ability, as shown in Fig. 5. Instead of treating the fission gas in each individual fuel tube (as in the SSR-W), the fission gas from the whole bulk fuel container of the inverted SSR can be collected and processed at once. This unique feature of the inverted SSR circumvents the fabrication of the hundreds of thousands of specially designed fuel tubes employed in the SSR-W, and is therefore expected to substantially decrease the capital cost of the reactor. The shape of the bulk fuel container employed in the inverted SSR can be specifically designed to serve different purposes (e.g., to enhance the cooling of certain areas), and was made cylindrical in this paper for a better neutron economy. The fuel container of the inverted SSR is fabricated with HT-9 steel. The wall thickness of the fuel container was assumed be 0.05 cm in this work (similar to the thickness of the cladding of the SSR-W), while optimization study on the wall thickness will be performed in future studies. The materials were defined exactly the same in the neutronics models of both reactor designs, and the cross-sectional area of the fuel material, the reactor pool, and the reflector/shielding were not modified such that the neutron economy can be directly reflected by the k_{eff} calculated. One viable core configuration of the inverted SSR consisted of ~ 71900 identical coolant channels, with a diameter of 0.715 cm each, evenly distributed in a cylindrical fuel tank with a diameter of ~ 165 cm (the determination of this core configuration will be discussed in more details in Section 3).

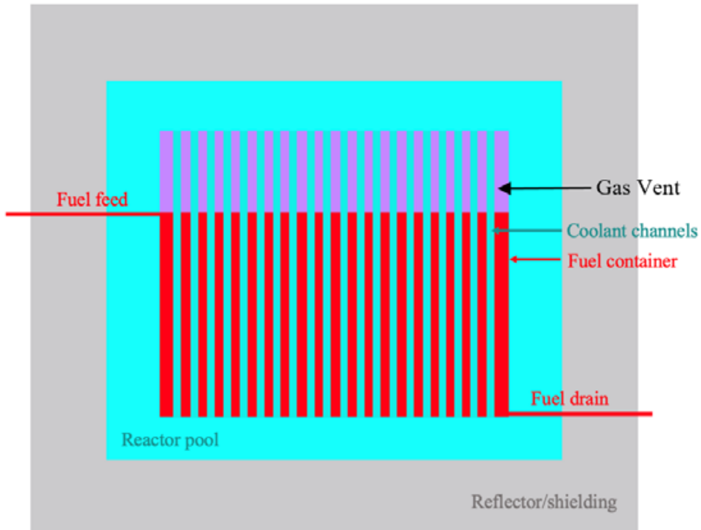

Figure 5. The configuration inside the inverted SSR core (side view).

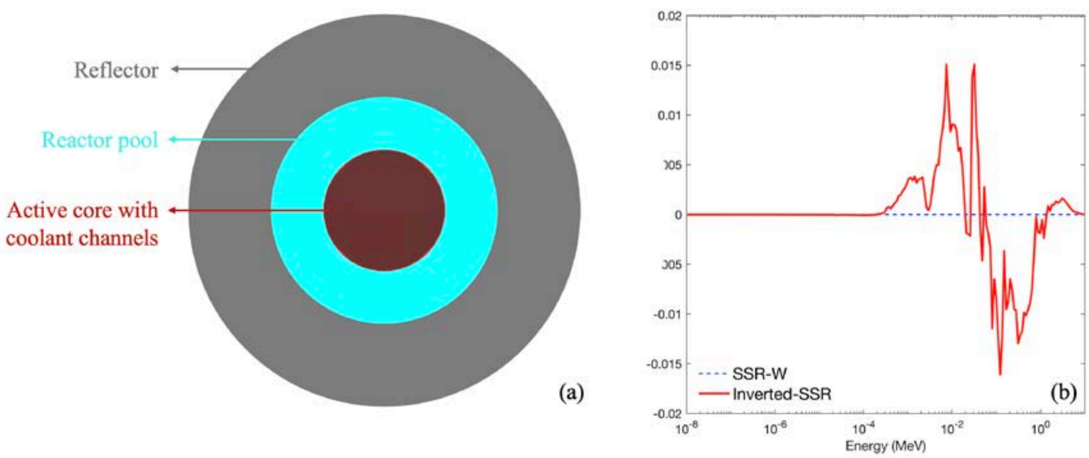

Figure 6. (a) The 2-D Serpent neutronics model of the inverted SSR (top view) and (b) the difference in the neutron spectra between the inverted SSR and the SSR-W.

The 2-D neutronics model of the inverted SSR core built in this work is shown in Fig. 6(a). The k_{eff} of the inverted SSR was calculated to be 1.44816 ± 0.00009, which was 370 pcm larger than that of the SSR-W. Although both reactors are fast-spectrum designs, the FLiBe, currently employed as the coolant, also works as the moderator to some extent due to the low atomic mass number of Fluoride. The moderator-to-fuel ratio in the active core of the inverted SSR was ~0.6 while that in the active core of the SSR-W was ~0.5. The higher moderator-to-fuel ratio led to a softer neutron spectrum, as shown in Fig. 6(b), and was another contributor to the superior neutron economy in the inverted SSR besides its cylindrical-shaped active core.

3. THERMAL-HYDRAULIC PERFORMANCE ANALYSIS

Apart from the superior neutron economy demonstrated in Section 2, a good cooling ability is also an important design criterium of the inverted SSR that needs to be met. In this section, preliminary thermal-hydraulics calculations were performed to both reactor designs to examine the maximum fuel temperature in the core during normal operating conditions with largely conservative assumptions. The superior cooling ability of the inverted SSR was demonstrated with the calculation results.

3.1. Maximum fuel temperature of the SSR-W

The temperature in the fuel rods of the SSR-W and the surrounding cladding was calculated by using the following two questions [14]:

$$T_{f,r} = T_{f,m} - \frac{q'''r^2}{4k_f}, \tag{3}$$

$$q' = \frac{2\pi k_c(T_{c,i} - T_{c,o})}{\ln(1 + b/a)}. \tag{4}$$

Eq. (3) was used for the fuel temperature calculation, where T_r was the fuel temperature at the radial location r $(0 \leq r \leq R)$, T_m was the fuel centerline temperature, q''' was the power density, and k_f was the fuel thermal conductivity. Eq. (4) was used for the cladding temperature calculation, where q' was the linear power, k_c was the thermal conductivity of the cladding, a was the inner radius of the cladding, b was the thickness of the cladding, $T_{c,i}$ and $T_{c,o}$ were the cladding temperature at the inner surface and the outer surface, respectively. To facilitate the analysis, the following assumptions were made in the calculation:

- The fuel was static and considered as solid in the temperature calculation, and the convection of fuel in each fuel rod was ignored. The fuel thermal conductivity, k_f, was $0.5 Wm^{-1}K^{-1}$ [4].
- The fuel temperature and the cladding temperature were equal at the point of contact ($T_R = T_i$).
- The cladding temperature at the outer surface, $T_{c,o}$, was equal to the coolant temperature at the outlet of the SSR-W, 630 ℃ [1].
- The cladding thermal conductivity, k_c, was $25.5 Wm^{-1}K^{-1}$ [15].

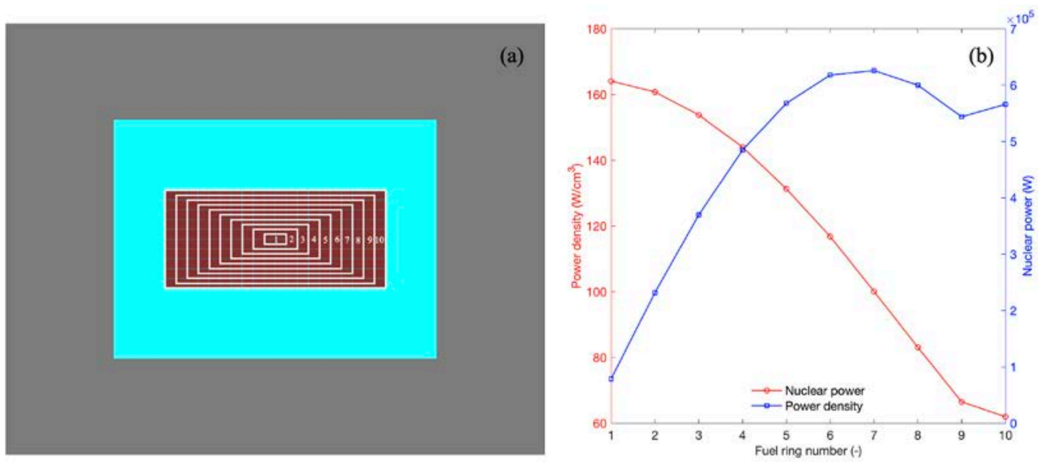

Figure 7. (a) The 10 fuel rings of the SSR-W and (b) the corresponding power distribution.

The active core of the SSR-W was divided into 10 concentric fuel rings with the same thickness, as shown in Fig. 7(a). The nuclear power was tallied in each ring of the 2-D neutronics model, and the power density (q''') and the linear power (q') were calculated accordingly, as shown in Fig. 7(b). The power density of the inner-most ring had the largest value ($164 W/cm^3$), as expected, and was considered for the calculation of the maximum fuel temperature. By plugging in all the parameters discussed above, the maximum fuel temperature of the SSR-W during normal operating condition was calculated as 2292 ℃. This very high temperature calculated (even higher than the boiling temperature, 1563 ℃, of the fuel salt [4]) was mainly caused by the extremely small fuel thermal conductivity when treated as a solid. However, convections of the molten fuel salt would occur, and the real fuel temperature should be significantly lower than the one calculated in this work. Despite the unrealistic nature of the calculated maximum fuel temperature of the SSR-W, it can be used as a reference to evaluate the thermal performance of the inverted SSR.

3.2. Maximum fuel temperature of the inverted SSR

Eq. (3) and Eq. (4) were not directly applicable to the inverted SSR as the bulk fuel container form was employed in the inverted SSR rather than fuel rods. Therefore, it was considered that the fuel container of the inverted SSR can be approximately represented by repeating the unit cell shown in Fig. 8(a), which was then converted to an equivalent fuel rod shown in Fig. 8(b). The cross-sectional areas of both the fuel and the cladding were conserved during the conversion, and Eq. (3) and Eq. (4) were then applied to the equivalent fuel rod for the temperature calculation. The parameters subject to change for the core configuration of the inverted SSR included the number of the coolant channels, the diameter of the coolant channel, and the pitch of the coolant channels. The cross-sectional area of the active core also changed accordingly such that the total amount of fuel was kept unchanged.

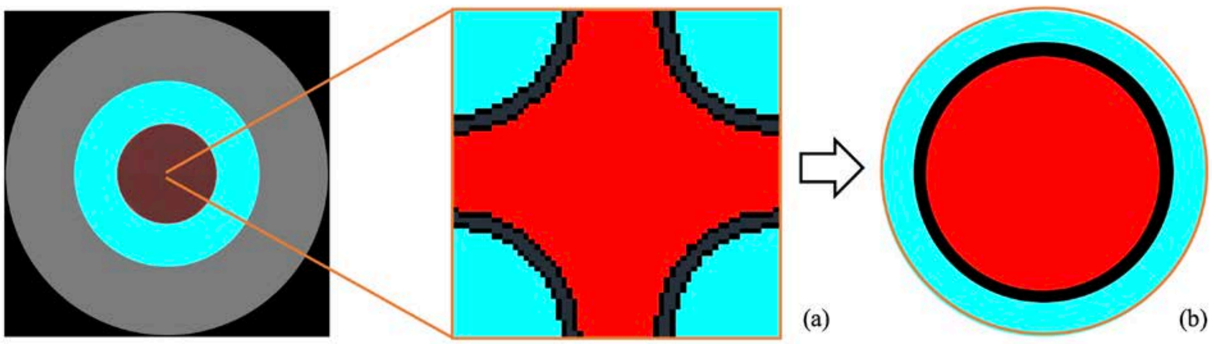

Figure 8. (a) The unit cell of the inverted SSR active core and (b) the equivalent fuel rod.

The centerline fuel temperature as a function of the equivalent radius of the fuel rod is plotted in Fig. 9 by assuming a power density of $160W/cm^3$ and a cladding thickness of 0.05 cm. Because the centerline (maximum) fuel temperature increases quadratically with the radius of the equivalent fuel rod, as suggested by both Fig. 9 and Eq. 3, it is essential to control the radius of the equivalent fuel rod so that the maximum fuel temperature is acceptable. The radius of the equivalent fuel rod was expected to be around 0.45 cm so that the maximum fuel temperature of the inverted SSR can be inferred to be around 2200 ℃.

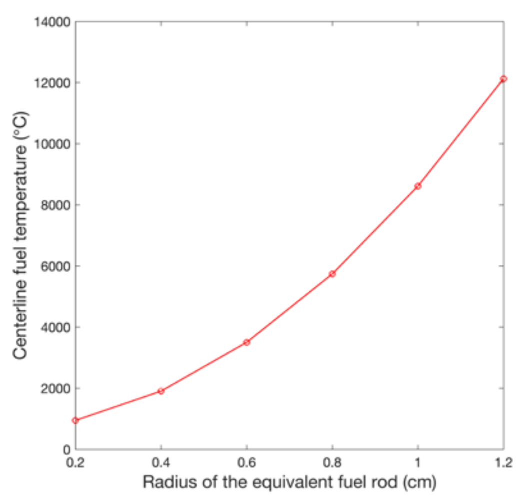

Figure 9. Centerline fuel temperature along the radius of the equivalent fuel rod.

To further assess the performance characteristics of the inverted SSR, various configurations of the design were envisioned and investigated in this study. All the assumptions and thermal properties formerly employed in the fuel temperature calculations were kept the same as those in the SSR-W analysis such that a direct comparison can be conducted. The active core of the inverted SSR was also divided into 10 concentric fuel rings with the same thickness, and the nuclear power of each fuel ring was tallied in the neutronics model. The largest power density was then employed for the calculation of the maximum fuel temperature in the inverted SSR. Important characteristics of the core configurations, including the number of the coolant channels, the diameter of the coolant channel, the pitch of the coolant channels, the cross-sectional area of the active core, the radius of the equivalent fuel rod, the k_{eff}, and the centerline fuel temperature, of seven example configurations are summarized in Table I.

Table I. Example inverted SSR core configurations and their characteristics

Config.	Number of coolant channels (-)	Diameter of coolant channels (cm)	Pitch of coolant channels (cm)	Radius of equivalent fuel rods (cm)	Radius of active core (cm)	k_{eff}	Max. fuel temp. (°C)
1	30884	1.5	1.625	0.448	187	1.32791	808
2	30884	1.0	1.625	0.733	157	1.53763	4868
3	69453	0.8	1.15	0.467	171	1.41605	2375
4	69453	0.76	1.14	0.478	168	1.44515	2575
5	69453	0.72	1.1	0.466	165	1.46043	2367
6	69453	0.7	1.15	0.511	164	1.51945	2687
7	71901	0.715	1.08	0.453	165	1.44816	2193

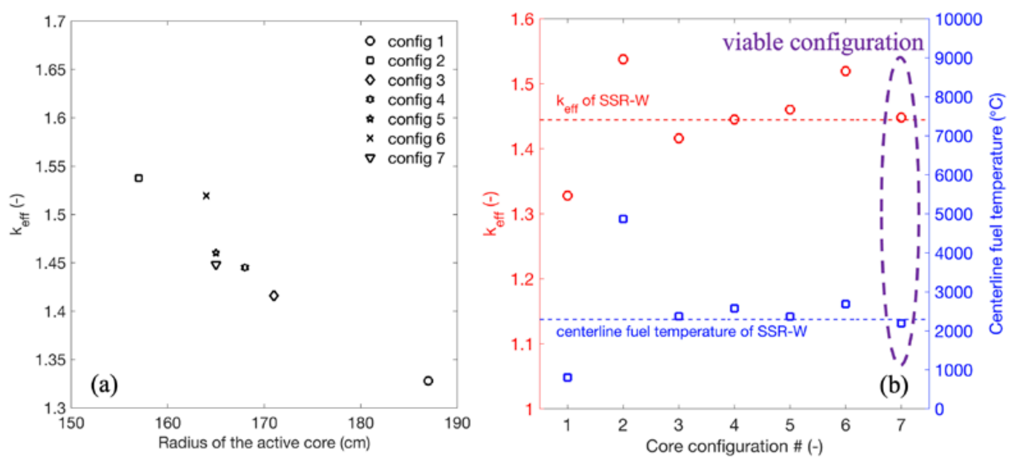

Figure 10. (a) k_{eff} as a function of the radius of the active core and (b) the k_{eff} and the maximum fuel temperature of the seven example inverted SSR core configurations.

The k_{eff} of the example core configurations as a function of the radius of the active core is plotted in Fig. 10(a), which suggested that apart from the shape of the active core and the neutron spectrum, the k_{eff} is also closely (negatively) correlated to the size of the active core. The negative correlation may be caused by a combined effect of both a hardened neutron spectrum and a higher neutron leakage but remains to be confirmed in our follow-up optimization study. The k_{eff} and the maximum fuel temperature of the inverted SSR of the seven example core configurations are plotted in Fig. 10 (b). Ingenious core configurations were required to get both a higher k_{eff} and a lower maximum fuel temperature at the same time as these two values tended to vary in the same direction. The configuration number 7, shown in Table I, was identified as one viable core configuration of the inverted SSR that can provide both a higher k_{eff} and a lower maximum fuel temperature than those of the SSR-W. Optimization studies should be performed in the future to further improve the performance of the inverted SSR. For example, instead of the even distribution of the coolant channels employed in this paper, the coolant channels can be located according to the cooling ability required (more coolant channels in the locations with higher power density) to further decrease the fuel temperature. Although the configuration number 7 of the inverted SSR was not optimized, it already demonstrated the superior performance of the inverted SSR.

4. CONCLUSIONS

This paper presented the preconceptual design of a novel inverted stable-salt reactor, the capital cost of which is expected to be substantially lower than the Moltex SSR-W design. One viable core configuration of the inverted SSR was identified in this study, and preliminary neutronics and thermal-hydraulics calculations were performed to demonstrate the superior performance of the inverted SSR. Many future investigations to the presented design can be carried out. For example, only normal operating conditions were considered in this study, and transient calculations are still needed to understand the core behavior during accidental scenarios. Moreover, detailed CFD calculations are needed to investigate the fluid flow inside the bulk fuel containment of the inverted SSR to have better ideas on how the convection can affect the fuel temperature. The understanding of the fluid flow inside the fuel containment is also indispensable for a reasonable depletion calculation. Additionally, the fabrication of the bulk fuel tank with almost 72,000 coolant channels may be challenging, even with the help of additive manufacturing technologies. Reasonable fuel container replacement strategies should also be developed in the future.

REFERENCES

1. IAEA, *Advances in small modular reactor technology developments 2018 Edition*, pp. 217-220, IAEA Advanced Reactors Information System (ARIS) (2018).
2. T. Jing, G. Yang, Y. S. Jung, and W. S. Yang, "Stationary Liquid Fuel Fast Reactor SLFFR–Part I: Core Design," *Nuclear Engineering and Design*, **310**, pp. 484-492 (2016).
3. J. Leppänen, M. Pusa, T. Viitanen, V. Valtavirta, and T. Kaltiaisenaho, "The Serpent Monte Carlo Code: Status, Development and Applications in 2013," *Ann. Nucl. Energy*, **82**, pp. 142-150 (2015).
4. T. J. Dolan, *Molten salt reactors and thorium energy*, pp. 571-580, Woodhead Publishing (2017).
5. O. W. Hermann et al., "Validation of the SCALE System for PWR Spent Fuel Isotopic Composition Analyses," Technical Report ORNL/TM-12667, Oak Ridge National Laboratory (1996).
6. B. Merk, A. Detkina, S. Atkinson, D. Litskevich, and G. Cartland-Glover, "Evaluation of the Breeding Performance of a NaCl-UCl-Based Reactor System," *Energies*, **12**, pp. 3853 (2019).
7. H. Q. Yin, J. Lin, B. Hu, W. G. Liu, X. F. Guo, Q. Liu, and Z. F. Tang, "Thermodynamic Description of the Constitutive Binaries of the NaCl-KCl-UCl3-PuCl3 System," *CALPHAD: Computer Coupling of Phase Diagrams and Thermochemistry*, **70**, pp. 101783 (2020).
8. S. K. Sahoo, V. N. Gaffney, A. Chatterjee, and K. L. Murty, "Annealing Behaviour of Ferritic HT-9 Steel," *Materials Science Forum*, **702-703**, pp. 794-797 (2012).
9. C. Zheng et al., "Effect of Dose on Irradiation-induced Loop Density and Burgers Vector in Ion-irradiated Ferritic/Martensitic Steel HT9," *Philosophical Magazine*, **98**(26), pp. 2440-2456 (2018).
10. M. R. Raza, F. Ahmad, M. A. Omar, R. M. German, and A. S. Muhsan, "Defect Analysis of 316LSS during the Powder Injection Moulding Process," *Defect and Diffusion Forum*, **329**, pp. 35-43 (2012).
11. J. S. Cagnone, K. Hillewaert, and N. Poletz, "Simulation of Non-Equilibrium Fusion Welding Using the Discontinuous Galerkin Method," (2015).
12. "The SSR- Safer, Cleaner, Cheaper," https://www.nuclearinst.com/write/MediaUploads/NI_webinar_-_Dr_Ian_Scott_-_MSRs.pdf, Accessed on July 11, 2021.
13. C. Lu, B. D. Hiscox, K. A. Terrani, and N. R. Brown, "Fully Ceramic Microencapsulated Fuel in Prismatic High Temperature Gas-Cooled Reactors: Analysis of Reactor Performance and Safety Characteristics," *Annals of Nuclear Energy*, **114**, pp. 277-287 (2018).
14. J. R. Lamarsh, *Introduction to Nuclear Engineering, 3rd ed.* pp. 423-425. Addison-Wesley, Prentice Hall, Upper Saddle River, New Jersey 07458, USA (1983).
15. L. Leibowitz and R.A. Blomquist, "Thermal Conductivity and Thermal Expansion of Stainless Steels D9 and HT9," *Int. J. Thermophys*, **9**(5), pp. 873-883 (1988).